Article

Chinese Science Bulletin

Engineering Thermophysics

February 2013 Vol.58 No.4-5: 567–574
doi: 10.1007/s11434-012-5463-x

Modeling cavitation flow of cryogenic fluids with thermodynamic phase-change theory

ZHANG XiaoBin, WU Zhao, XIANG ShiJun & QIU LiMin*

Institute of Refrigeration and Cryogenic Engineering, Zhejiang University, Hangzhou 310027, China

Received February 19, 2012; accepted July 26, 2012

Cavitation is the formation of vapor bubbles within a liquid where the flow dynamics causes the local static pressure to drop below the vapor pressure. The so-called full cavitation model (FCM) developed by Singhal has been widely used in numerical modeling of the cavitation flow for thermosensible and non-thermosensible fluids. Within the FCM, the bubble size is taken to be equivalent to the maximum possible value to forego the calculation of bubble number density. We developed a new cavitation model by re-calculating the bubble radius in FCM to account for the effects of local pressure. The new model was obtained by combining the thermodynamic phase-change theory and the Young-Laplace equation with the assumption of thermodynamic equilibrium during the cavitation process. The cavitation calculations were performed based on the mathematical framework of the homogeneous equilibrium flow model and the transport-equation-based model for vapor phase mass fraction. The model was validated by modeling the cavitating flow of liquid nitrogen and liquid hydrogen through NASA hydrofoil and Ogive with consideration of the phase-change thermal effects. The temperature and pressure distributions with the new model are found to agree well with data from existing experimental studies, as well as the simulations with the FCM.

cavitation, CFD, cryogenic, phase-change

Citation: Zhang X B, Wu Z, Xiang S J, et al. Modeling cavitation flow of cryogenic fluids with thermodynamic phase-change theory. Chin Sci Bull, 2013, 58: 567–574, doi: 10.1007/s11434-012-5463-x

The cavitation phenomenon happens in a liquid when the local static pressure drops below the vapor pressure, where the generated vapor sustains the pressure dynamic balance. Cavitation can be observed in a wide variety of propulsion and power systems such as inducers, pumps, turbines, nozzles, hydrofoils, slip bearings, etc. [1]. In most cases, cavitation is unavoidable and undesirable, and is a major source of noise, vibration, and erosion in hydraulic mechanical systems [2]. To understand and predict the effects of cavitation, a robust cavitation model is desired for the computational modeling of complex two-phase issues.

Efforts have been made to model cavitating flow with the homogenous equilibrium flow model (HEFM), in which the single-fluid modeling approach is employed for both phases [3–10]. The key for implementation of the HEFM is to calculate the variable density field. Wang et al. [11] and Wu et al. [12] have reviewed these calculation models in detail. Among the various modeling approaches, the transport equation-based cavitation models (TEM) have been widely used recently [6–12]. The TEM solves the transport equation of vapor volume (or mass) fraction, whose source terms are the condensation and evaporation rate in the liquid-vapor conversion. Commonly used cavitation models for calculating these phase transformation rates are summarized in Table 1 in chronological order of publication date [1,7,13,14]. The first two models largely depend on empirical judgment with much uncertainty to cavitation of various fluids. The third model-the so called "full cavitation model" (FCM)-has been proven to be capable of modeling isothermal [1] as well as cryogenic fluid cavitation [9,10,15], and has been adopted by the commercial CFD software package Fluent [16]. However, this model assumes the bubble radius to be the maximum possible value during the cavitation processes, and ignores the effects of local pressure on bubble size. Therefore,

*Corresponding author (email: Limin.qiu@zju.edu.cn)

Table 1 Source terms in cavitation models in CFD studies [1,7,13,14]

Authors	Production term-m^+	Destruction term-m^-
Singhal et al. (1997) Merkle et al. (1998)	$\frac{C_{\text{prod}}\text{MAX}(p-p_\text{v},0)(1-\alpha_\text{l})}{(0.5\rho_\text{l}U_\infty^2)t_\infty}$, C_{prod}=80	$\frac{C_{\text{liq}}\rho_\text{l}\text{MIN}(p-p_\text{v},0)\alpha_\text{l}}{(0.5\rho_\text{l}U_\infty^2)\rho_\text{v}t_\infty}$, C_{liq}=1
Kunz et al. (2000)	$\frac{C_{\text{prod}}\alpha_\text{l}^2(1-\alpha_\text{l})}{\rho_\text{l}t_\infty}$, $C_{\text{prod}}=3\times10^4$	$\frac{C_{\text{liq}}\rho_\text{v}\text{MIN}(p-p_\text{v},0)\alpha_\text{l}}{(0.5\rho_\text{l}U_\infty^2)\rho_\text{l}t_\infty}$, C_{liq}=1
Singhal et al. (2002)	$\frac{C_{\text{prod}}\sqrt{k}}{\sigma}\rho_\text{l}\rho_\text{v}\left[\frac{2}{3}\frac{\text{MAX}(p-p_\text{v},0)}{\rho_\text{l}}\right]^{1/2}$, C_{prod}=0.02	$\frac{C_{\text{liq}}\sqrt{k}}{\sigma}\rho_\text{l}\rho_\text{l}\left[\frac{2}{3}\frac{\text{MAX}(p-p_\text{v},0)}{\rho_\text{l}}\right]^{1/2}$, C_{liq}=0.01
Senocak and Shyy (2004)	$\frac{\text{MAX}(p-p_\text{v},0)(1-\alpha_\text{l})}{(V_{\text{v,n}}-V_{\text{l,n}})^2(\rho_\text{l}-\rho_\text{v})t_\infty}$	$\frac{\rho_\text{l}\text{MIN}(p-p_\text{v},0)\alpha_\text{l}}{\rho_\text{v}(V_{\text{v,n}}-V_{\text{l,n}})^2(\rho_\text{l}-\rho_\text{v})t_\infty}$

the accuracy of modeling unsteady cavitation with this model is questionable. The last model was developed by relying on interfacial mass and momentum transfer properties, and its usage extends to unsteady cavitation. However, it is not yet empiricism-free in computing the velocity perpendicular to the gas/liquid interface.

The present paper introduces a new cavitation model, named the "dynamic cavitation model" (DCM), in which we re-calculate the bubble size in FCM by taking the effect of local pressure into account. The model combines the classical thermodynamic phase-change theory and Young-Laplace equations under the assumption of thermodynamic equilibrium during the cavitation process. The thermodynamic equilibrium assumption for LN_2 and LH_2 cavitation modeling was validated by Hosangadi and Ahuja [8]. Afterwards, the model was implemented as a resource term into transport equations of the gas mass fraction, which were solved together within the mathematical framework of the homogeneous equilibrium model in multiple-phase CFD calculations. The validation of this model was made by modeling the quasi-steady cavitating flow through the NASA hydrofoil and Ogive, and comparing the temperature and pressure profiles with available experimental data in Hord's reports [17,18] as well as computational results of FCM. We find that the dynamic cavitation model is at the same precision level as the full cavitation model.

1 Cavitation equations based on the mixture model

The set of governing equations for cavitation based on the HEFM comprises the conservative form of the Navier-Stokes equations, the energy equation, the κ-ε two-equation turbulence closure, and a transport equation for the vapor mass fraction. The continuity, momentum, and energy equations for steady flow are given below, respectively [12]:

$$\frac{\partial(\rho_\text{m}u_j)}{x_j}=0, \tag{1}$$

$$\frac{\partial(\rho_\text{m}u_iu_j)}{\partial x_j}=-\frac{\partial P}{\partial x_i}+\frac{\partial}{\partial x_j}\left[(\mu+\mu_t)\left(\frac{\partial u_i}{\partial x_j}+\frac{\partial u_j}{\partial x_i}-\frac{2}{3}\frac{\partial u_k}{\partial x_k}\delta_{ij}\right)\right], \tag{2}$$

$$\frac{\partial}{\partial x_j}(\rho_\text{m}u_jT)=\frac{\partial}{\partial x_j}\left[(k+k_\text{t})\frac{\partial T}{\partial x_j}\right]+S_\text{E}, \tag{3}$$

where x and the indices i, j and k denote the coordinate axes, t is time, ρ_m is the mixture density, defined as, $\rho_\text{m}=\rho_\text{v}\alpha_\text{v}+\rho_\text{g}\alpha_\text{g}+\rho_\text{l}(1-\alpha_\text{v}-\alpha_\text{g})$ (hereafter, the subscript m for all mixture variants will be omitted for brevity), α represents the volume fraction, and the subscripts v, g and l denote, respectively, the vapor phase, non-condensable gas, and liquid phase, u represents the velocity vector, P is pressure, T is temperature, μ is viscosity, and the subscript t denotes turbulent flow, k is thermal conductivity, S_E is the volumetric heat sources calculated by the product of the phase change rate and the latent heat. The effect of slip velocity between the liquid and vapor phases on the momentum exchange has been neglected in eq. (2) because cavitation often occurs in regions of high-speed flow. The effect of compressible work and viscous dissipation on energy conservation is ignored in eq. (3) because the temperature field in cryogenic cavitation is mainly dictated by evaporative cooling. Time derivative terms in these equations have been dropped for steady flow computations.

The κ-ε two-equation turbulence model has been widely used in simulating the quasi-steady cavitating flow of cryogenic fluids [8,12,19]. Compared with the standard κ-ε model, the realizable κ-ε turbulence model has shown substantial improvements in computing flows with sharp streamline curvature or vortices. In regards to the near- wall treatment effects, the present author's previous studies have shown that both the standard wall function (SWF) and the enhanced wall treatment (EWT) can produce matching results compared with experimental data [20]. Therefore, we employ the realizable κ-ε model to investigate turbulent mixing, and SWF to account for boundary layer effects, whose

detailed formulations are detailed in [16].

2 Theoretical deduction of dynamic cavitation model

The vapor mass fraction f in a cavitation process is determined by solving the transport equation for steady calculations as follows:

$$\nabla\cdot\left(f\rho u_{\mathrm{v}}\right)=\dot{R}\,, \tag{4}$$

where R is the net evaporation or condensation rate, depending on the system. Singhal has utilized the Rayleigh-Plesset equation for bubble dynamics to deduce an expression for R as [1]:

$$\dot{R}=\left(n4\pi\right)^{1/3}\left(3\alpha_{\mathrm{v}}\right)^{2/3}\frac{\rho_{\mathrm{l}}\rho_{\mathrm{v}}}{\rho}\left[\frac{2}{3}\left(\frac{P_{\mathrm{b}}-P}{\rho_{\mathrm{l}}}\right)\right]^{1/2}, \tag{5}$$

where α_{v} is the vapor volume fraction and n is the bubble number density. In eq. (5), there is only one unknown parameter, n, on the right hand side needed in calculations of R, which can be transformed to the unknown bubble radius, $\Re_{\mathrm{b}}$:

$$\alpha_{\mathrm{v}}=n\frac{4}{3}\pi\Re_{\mathrm{b}}^{3}\,. \tag{6}$$

Singhal deduced the expression of FCM by using the maximum possible bubble radius, $\Re_{\mathrm{b}}=\dfrac{0.061We\sigma}{2\rho_{\mathrm{l}}u_{\mathrm{rel}}^{2}}$, which is determined by the balance between aerodynamic drag and surface tension, and commonly used in the nuclear industry. We is the Weber number, $We=\rho_{\mathrm{l}}u_{\mathrm{rel}}^{2}L_{\mathrm{ch}}/\sigma$, σ is surface tension, and u_{rel} is the relative velocity between the two phases. It should be noted that the expression for $\Re_{\mathrm{b}}$ is independent of the local pressure, which is a potentially improper way to explain the dynamic nature of the cavitation process (the bubble periodically grows and detaches from the wall, especially for cloud and vortex cavitation). The Rayleigh-Plesset bubble dynamic equation [21] also explicitly indicates that local pressure changes have substantial effects on the bubble size. Although the FCM behaves well in modeling quasi-steady cavitation [1,9,20], where local pressure as well as the time-averaged bubble radius is nearly invariable, its feasibility for modeling unsteady cavitations has yet to be carefully verified.

The classical thermodynamic phase-change theory provides a way to calculate the variable bubble radius [21]. If the liquid phase and vapor phase reach thermodynamic equilibrium in a short time interval during the cavitation process, the temperature and chemical potential in the vapor and the liquid should be equal:

$$T_{\mathrm{v}}=T_{\mathrm{l}}\,,\quad \mu_{\mathrm{v}}=\mu_{\mathrm{l}}\,. \tag{7}$$

The pressure of the vapor and liquid phases are related by the Young-Laplace equation as follows:

$$P_{\mathrm{v}}=P_{\mathrm{l}}+2\sigma/\Re_{\mathrm{b,e}}\,, \tag{8}$$

where the subscript e represents the equilibrium state. By ignoring the thermodynamic effect and assuming isothermal phase change, we obtain the integral form of the Gibbs-Duhem equation [21] from $P=P_{\mathrm{sat}}$ to any arbitrary pressure P:

$$\mu\text{-}\mu_{\mathrm{sat}}=\int_{P_{\mathrm{sat}}}^{P}v\mathrm{d}P\,, \tag{9}$$

where subscript sat denotes the saturation state. For an ideal gas, this yields the following relation for the chemical potential of the vapor and its equilibrium pressure $P_{\mathrm{v,e}}$:

$$\mu_{\mathrm{v}}=\mu_{\mathrm{sat,v}}+\mathrm{R}T_{\mathrm{l}}\ln\left[\frac{P_{\mathrm{v,e}}}{P_{\mathrm{sat}}\left(T_{\mathrm{l}}\right)}\right]. \tag{10}$$

For the liquid phase, eq. (10) can be reduced easily to eq. (11) because of incompressibility:

$$\mu_{\mathrm{l}}=\mu_{\mathrm{sat,l}}+v_{\mathrm{l}}\left[P_{\mathrm{l}}-P_{\mathrm{sat}}\left(T_{\mathrm{l}}\right)\right]. \tag{11}$$

Substituting eqs.(10) and (11) into the required equilibrium condition of eq. (7), and using the fact that $\mu_{\mathrm{sat,v}}=\mu_{\mathrm{sat,l}}$, the following relation is obtained:

$$P_{\mathrm{v,e}}=P_{\mathrm{sat}}\left(T_{\mathrm{l}}\right)\exp\left\{\frac{v_{\mathrm{l}}\left[P_{\mathrm{l}}\text{-}P_{\mathrm{sat}}\left(T_{\mathrm{l}}\right)\right]}{\mathrm{R}T_{\mathrm{l}}}\right\}. \tag{12}$$

For superheated liquids, P_{l} must be less than $P_{\mathrm{sat}}\left(T_{\mathrm{l}}\right)$; consequently, the term in braces in eq. (12) is less than zero and $P_{v,e}$ is less than $P_{\mathrm{sat}}\left(T_{\mathrm{l}}\right)$. Substituting eq. (12) into eq. (8), the following relation for $\Re_{\mathrm{b,e}}$ is obtained:

$$\Re_{\mathrm{b,e}}=\frac{2\sigma}{P_{\mathrm{sat}}\left(T_{\mathrm{l}}\right)\exp\left\{\left[P_{\mathrm{l}}-P_{\mathrm{sat}}\left(T_{\mathrm{l}}\right)\right]/\left(\rho_{\mathrm{l}}\mathrm{R}T_{\mathrm{l}}\right)\right\}-P_{\mathrm{l}}}. \tag{13}$$

Similarly, the same principle applies to the correlation between bubble radius $\Re_{\mathrm{b,e}}$ and pressure in condensation process [21]:

$$\Re_{\mathrm{b,e}}=\frac{2\sigma}{\rho_{\mathrm{l}}\mathrm{R}T_{\mathrm{v}}\ln\left[P_{\mathrm{v}}/P_{\mathrm{sat}}\left(T_{\mathrm{v}}\right)\right]-P_{\mathrm{v}}+P_{\mathrm{sat}}\left(T_{\mathrm{v}}\right)}. \tag{14}$$

Here, P_{l} and P_{v} in eqs. (13) and (14) are equal to the local pressure P. T_{l} and T_{v} are equal to the local temperature T during the CFD calculations.

After substituting eq. (6) into eq. (5), we get the expression for R unrelated to n:

$$\dot{R}=\frac{3\alpha_{\mathrm{v}}}{\Re_{\mathrm{b,e}}}\frac{\rho_{\mathrm{l}}\rho_{\mathrm{v}}}{\rho}\left(\frac{2}{3}\frac{P_{\mathrm{b}}-P}{\rho_{\mathrm{l}}}\right)^{1/2}. \tag{15}$$

By combining eqs. (13)–(15), and obtaining the vapor

volume fraction α_v through the correlation: $\alpha_v = f\rho/\rho_v$, we get the evaporation and condensation rate as follows, and consider that the phase change mass is proportional to the source phase volume fraction:

when $P_{sat}>P$ (evaporation process)

$$\dot{R}_e = C_e \frac{P_{sat}(T)\exp\left\{\left[P-P_{sat}(T)\right]/\left(\rho_l RT\right)\right\}-P}{\sigma} \times\rho_v\left(\frac{2}{3}\frac{P_{sat}-P}{\rho_l}\right)^{1/2}\left(1-f_v-f_{gas}\right), \quad (16)$$

when $P_{sat}\leqslant P$ (condensation process)

$$\dot{R}_c = C_c \frac{\rho_l RT\ln\left[P/P_{sat}(T)\right]+P_{sat}(T)-P}{\sigma} \times\rho_l\left(\frac{2}{3}\frac{P-P_{sat}}{\rho_l}\right)^{1/2} f_v, \quad (17)$$

where C_e and C_c are empirical constants and $f_{gas}=10^{-8}$ is fixed in our simulations to avoid the effects of non-condensable gases dissolved in the liquid. There is no assumption that the bubble pressure is equal to the saturation pressure in derivation of the bubble radius expression. However, those two pressures are practically very close in regard to thermodynamic theory, which means eqs. (16) and (17) can be further simplified. It is also seen that the bubble radius during phase change is a function of local pressure and saturation pressure. In isothermal cavitation like water, saturation pressure and surface tension are both constant, thus bubble radius only depends on local pressure. For an evaporation process, the evaporation rate increases when the local pressure P decreases; for condensation process, condensation rate is larger if local pressure P is higher.

The effects of turbulence on the cavitation are considered as FCM [1] by simply raising the phase-change threshold pressure value as:

$$P_{cav} = \left[P_{sat}(T)+P_t\right]/2, \quad (18)$$

where $P_t = 0.39\rho\kappa$ is turbulent pressure and subscript t means turbulence. Thus, eqs. (16) and (17) transform to:

when $P_{cav}>P$ (evaporation process)

$$\dot{R}_e = C_e \frac{P_{cav}(T)\exp\left\{\left[P-P_{cav}\right]/\left(\rho_l RT\right)\right\}-P}{\sigma} \times\rho_v\left(\frac{2}{3}\frac{P_{cav}-P}{\rho_l}\right)^{1/2}\left(1-f_v-f_{gas}\right), \quad (19)$$

when $P_{cav}\leqslant P$ (condensation process)

$$\dot{R}_c = C_c \frac{\rho_l RT\ln\left(P/P_{cav}\right)+P_{cav}-P}{\sigma}\cdot\rho_l\left(\frac{2}{3}\frac{P-P_{cav}}{\rho_l}\right)^{1/2} f_v. \quad (20)$$

Eqs. (1)–(4), (19), and (20) comprise the complete set of equations needed to describe turbulent cavitation. The CFD software Fluent6.3 [16] is employed to solve the set of equations, among which the continuity, momentum, and energy equations are simultaneously solved. The convective and diffusive terms are discretized using the second-order accurate upwind scheme and second-order accurate central scheme, respectively. The vapor mass fraction equation was implemented with the "QUICK" scheme. We considered that the convergence criteria in the calculations had been met when a three orders of magnitude drop in the momentum and vapor transfer equations and six orders in energy equation was achieved. However, only a two orders of magnitude drop in the mass conservation equation could be observed.

It was assumed that the phase change process of cavitation in liquid nitrogen and liquid hydrogen occurs at local thermodynamic equilibrium [8]. Hence, the thermodynamic properties of both the liquid and vapor phase, including the density, vapor pressure, viscosity, specific heat, and latent heat, etc., are functions of only temperature. The databank software "Gaspak 3.2" was used to generate these functions.

3 Simulations of hydrofoil cavitation

The Hord group from NASA has performed subscale tests of cryogenic liquids, e.g. liquid nitrogen and liquid hydrogen, cavitating flow around hydrofoil and Ogive in a blow-down tunnel. Their work represents the most comprehensive experimental data of pressure and temperature fields in the cavitation region, and sets the benchmark for verifying the cavitation model in our CFD study [17,18]. Details of the tunnel and hydrofoil geometry, as well as the calculation domain are given in Figure 1. The tunnel width is 25.4 mm while the hydrofoil width is 7.92 mm. A 2D model with multi-block quadrilateral grid scheme is adopted for the tunnel and hydrofoil. The entire flow field is covered by over 100000 grids, and the grids near the hydrofoil wall are specifically refined to guarantee $y+<100$, where $y+$ is the non-dimensional distance between the wall and the first cell centroid. In our previous study, the grid solutions were shown to provide grid-independent solutions [20]. Two cases for liquid nitrogen and one for liquid hydrogen in Hord's experiments were randomly selected and simulated, for which the boundary conditions are listed in Table 2 with the adiabatic tunnel walls. It should be pointed out that the backpressure was not specified by Hord's reports and thus

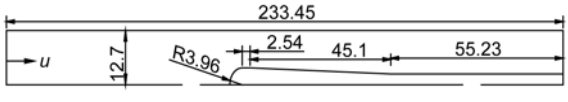

Figure 1 Geometry of tunnel and hydrofoil used by Hord [17] and the corresponding calculation domain.

Table 2 Boundary conditions for hydrofoil CFD modeling [17]

Liquids	No. (in original reports)	Inlet velocity (m/s)	Inlet temperature (K)	Inlet total pressure (Pa)	Outlet temperature (K)
LN_2	283C	14.5	77.71	211241.8	77.71
	284D	23.5	77.6	356795.2	77.6
LH_2	229C	40.4	20.62		20.62

was approximately calculated based on the mass conservation law and Bernoulli's equation in our CFD simulations.

The simulation results employing DCM and FCM are shown in Figures 2 and 3, respectively, along with the experimental data. After considering large numbers of permutations and combinations to produce the most consistent

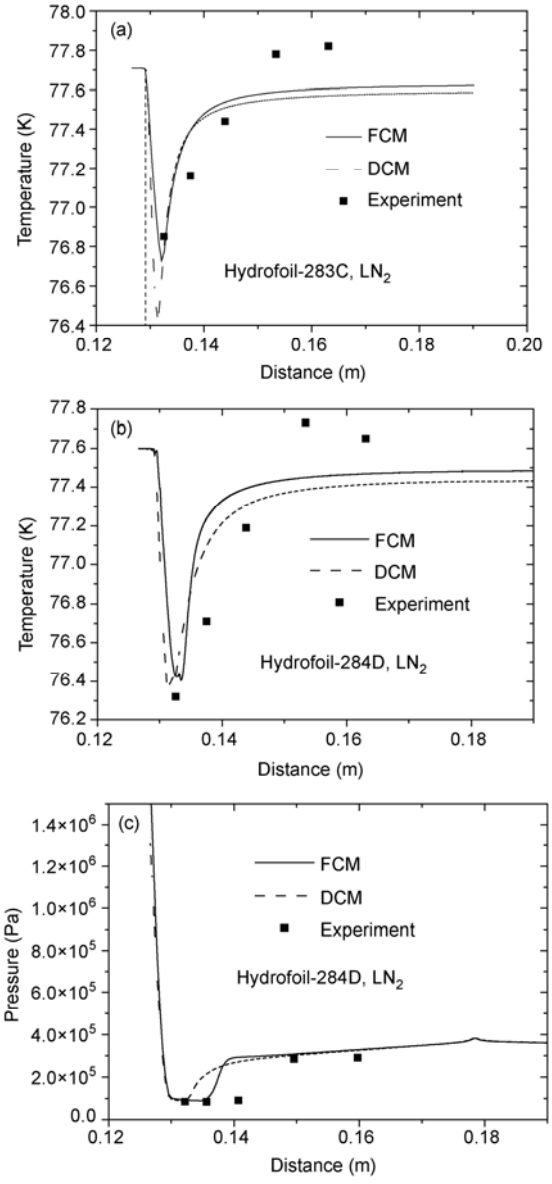

Figure 2 Temperature (a), (b) and pressure (c) distributions along the hydrofoil wall for liquid nitrogen cavitating flow.

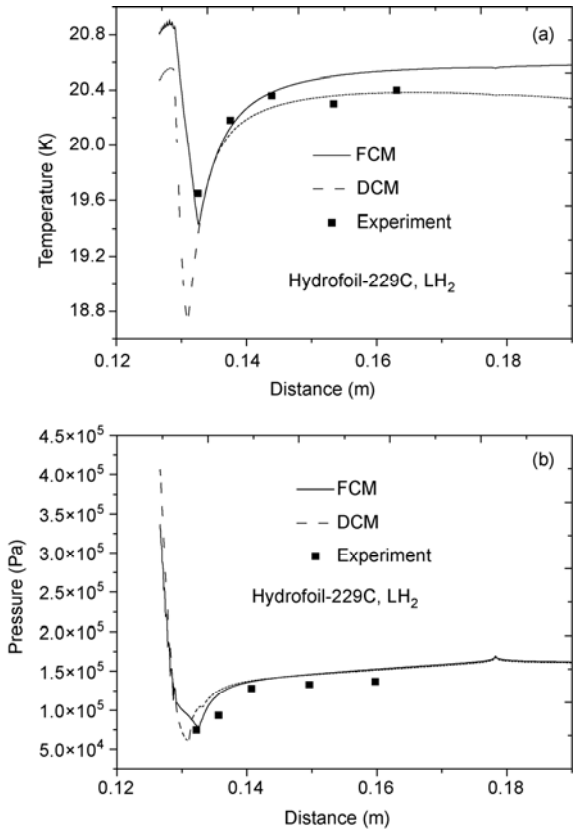

Figure 3 Temperature (a) and pressure (b) distributions along the hydrofoil wall for liquid hydrogen cavitating flow.

results of pressure and temperature distributions with the experimental data [17,18], the empirical constants in DCM were chosen to be C_e=0.018, C_c=0.01 for liquid nitrogen, and C_e=0.01, C_c=0.01 for liquid hydrogen. It is seen in the figures that the simulated results with the two models both agree well with the experimental data in most cavitation regions, considering the instrumentation uncertainty of 6900 Pa for pressure and 0.2 K for temperature [17,18]. Additionally, the computed pressure and temperature fields from these two models are also in good agreement. The dynamic nature of cavitation (bubble generation, expansion, and extinguishing) shows a fluctuating pattern in the size of the cavitation zone and the lowest temperature during the quasi-steady computations [11,22]. The amplitude of temperature vacillation is found to be about 0.3 K in our cases. From this viewpoint, we believe that DCM and FCM can reach the same precision level in 2D simulations for the hydrofoil. A discontinuity in pressure profiles appeared at about x=0.18 m in Figures 2 and 3 and is a result of the geometrical discontinuity, as shown in Figure 1, where is the junction with the trailing edge of the hydrofoil and the tunnel wall. It was observed that the temperature drop lags behind the pressure drop, which implies that the temperature is controlled by the evaporative cooling effects for thermosensible fluids. Therefore, the steep temperature and pressure curves at the leading edge of the hydrofoil in Figures 2 and 3 indicate

that the exchange between static and dynamic pressures has a dominant impact on the cavitation.

In the cavity closure region (approximately denoted by the last two experimental points in Figure 2), the temperatures from the two models both demonstrate a distinct difference compared with experiments: the simulated temperature does not recover to the inlet free-stream level and the tested temperature is evidently higher than the simulated values – even higher than the inlet value. The reason for this discrepancy is related to the mathematical formulation of the HEFM, in which only time-averaged physical quantities, especially the turbulent viscosity of the liquid and vapor phase in one cell are calculated [8].

4 Simulations of Ogive cavitation

The tunnel and Ogive geometry in the Hord group's cavitation experiments, as well as the calculation domain, is shown in Figure 4. The tunnel diameter is 16.76 mm while the Ogive diameter is 5.33 mm. The CFD geometric model is axial symmetric. The entire flow field is covered by over 53000 grids. As the treatment of hydrofoil, the grids near the walls are specifically refined to guarantee y^+<100. Also, two cases from Hord's experiments for liquid nitrogen and one for liquid hydrogen were randomly selected and simulated, of which the boundary conditions are listed in Table 3 with the adiabatic tunnel walls.

The simulated results employing DCM and FCM are shown in Figures 5 and 6, along with Hord's experimental data. Considering the instrumentation uncertainty, the temperature profiles from both cavitation models match the experimental data well. Because of the blockage effect of the tunnel wall, the measured temperature distributions along the Ogive wall seem disorderly, a feature which is also well captured by the simulations with DCM. It was found that the minimum pressure values with both models at the leading edge of the cavitation zone agree well with

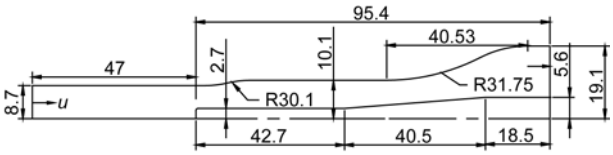

Figure 4 Geometry of tunnel and Ogive used by Hord [18] and the corresponding calculation domain.

Table 3 Boundary conditions for Ogive CFD modeling [18]

Liquids	No.(in original reports)	Inlet velocity (m/s)	Inlet temperature (K)	Inlet total pressure (Pa)	Outlet temperature (K)
LN_2	419A	14.9	83.75	212402.6	83.75
	420D	21.7	83.95	228243.5	83.95
LH_2	390B	66	21.87	165500	21.87

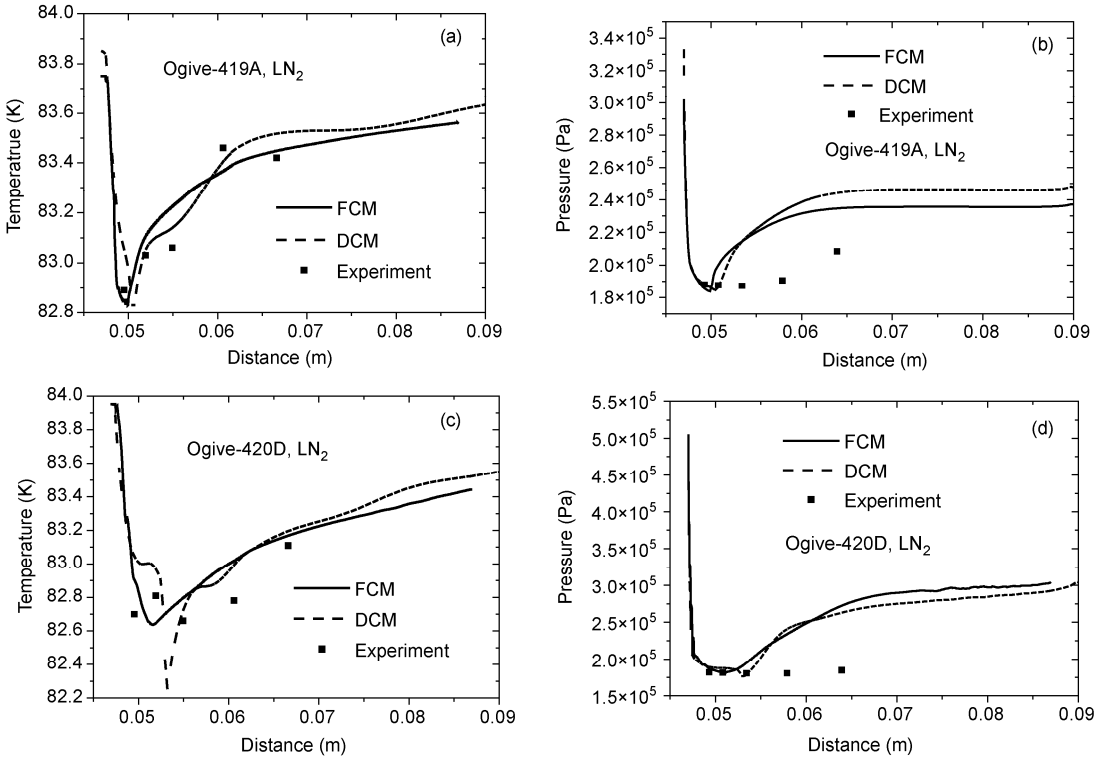

Figure 5 Temperature and pressure distributions along the Ogive wall for liquid nitrogen cavitating flow.

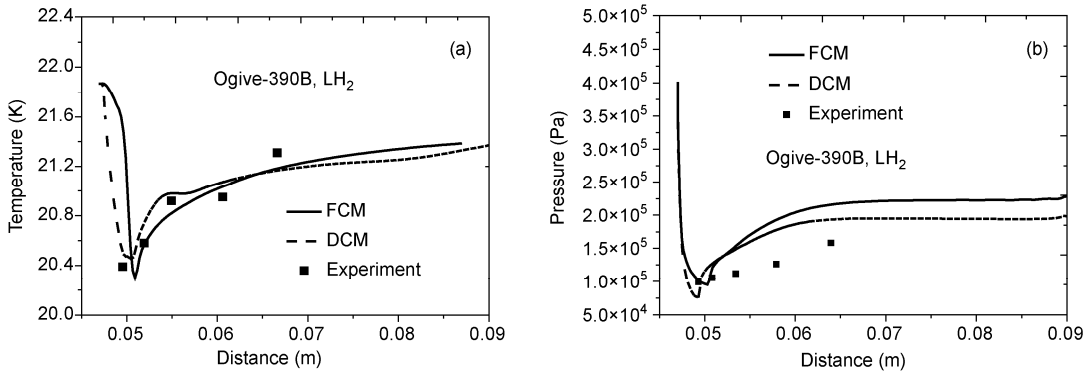

Figure 6 Temperature (a) and pressure (b) distributions along the Ogive wall for liquid hydrogen cavitating flow.

the experimental data. However, the pressure distributions at the cavitation closure zone significantly deviate from the experiments. Compared with the corresponding cases of hydrofoil simulations, differences exist in the geometrical configurations. Therefore, we also primarily attribute these deviations to blockage effects of the tunnel wall. However, the full mechanistic details which give rise to these deviations are not yet clear and understanding these details calls for further studies.

5 Discussion

Figures 7 and 8 show the simulated temperature contours for liquid hydrogen flow through hydrofoil-229C and liquid nitrogen flow through Ogive-419A with FCM and DCM. The pressure contour for hydrofoil-229C is presented in Figure 9. The particle traces of the fluid streamlines near the cavitation wall are also plotted. Simulations with the two models both reveal the cavitation mechanism of cryogenic fluids. For non-thermosensible liquids such as water, there exists a distinct gas/liquid interface and the liquid cannot flow into the cavity, which is sustained by the thermal diffusion across the gas/liquid interface [8]. However, for thermosensible liquids, the cavity is primarily sustained by the convective liquid, which can pierce into the cavity. More detailed explanations can be found in [6,8,9]. It is revealed by the figures that the simulated starting location of cavitation with DCM is ahead of that with FCM for all cases, which is because of the effects of local pressure on the bubble radius. As a result, the simulated temperature depression with DCM influences much larger areas of the cavitation zone than that with FCM.

6 Conclusions

Upon noticing that bubble radius was independent of the local pressure in the full cavitation model, we have developed a new cavitation model that considers the pressure-

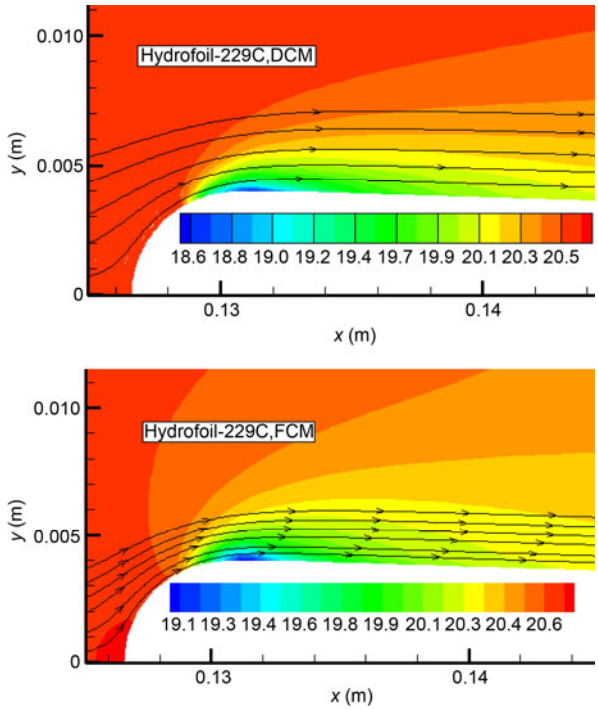

Figure 7 Temperature contours of liquid hydrogen flow through Hydrofoil-229C with FCM and DCM

dependent bubble radius. The model comprises the classical thermodynamic phase-change theory and the Young-Laplace equation with the assumption of thermodynamic equilibrium. The effect of surface tension on the bubble radius was also considered. CFD simulations were conducted on cavitation for liquid nitrogen and liquid hydrogen around NASA hydrofoil and Ogive designs. The results for both geometries were in good agreement with the full cavitation model and the experimental data. The new model can perform as precisely as the full cavitation model in computing temperature and pressure fields of quasi-steady cryogenic cavitation.

The new model adopts a local pressure-related bubble radius, and has the potential to allow computational study of unsteady cavitation. As in other reported cavitation models, thermodynamic effects are still ignored by the cavitation

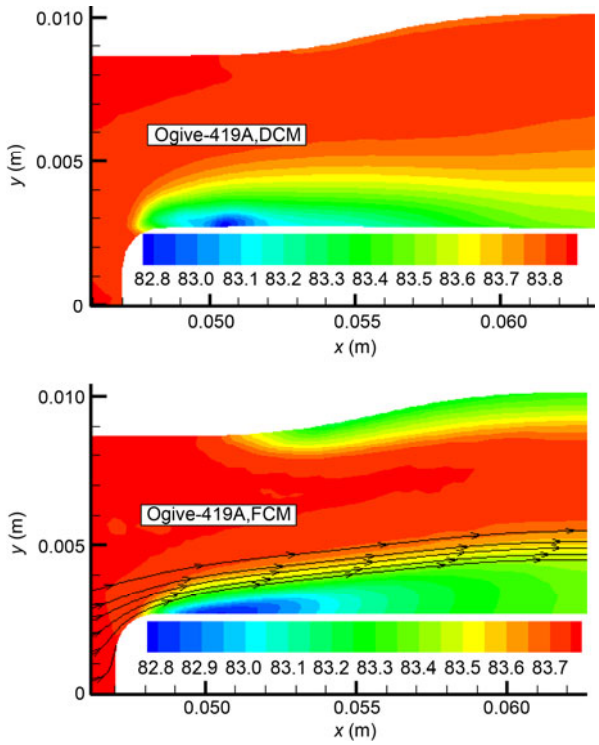

Figure 8 Temperature contours of liquid nitrogen flow through Ogive-419A.

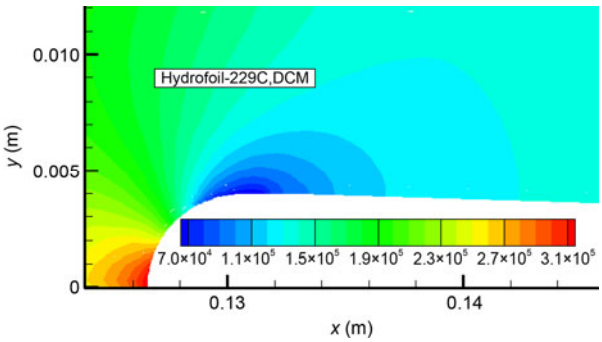

Figure 9 Pressure contour of liquid hydrogen through Hydrofoil-220C with DCM.

model itself (see eq. (9)), which is a good approximation for non-thermosensible fluids whose liquid/vapor density ratio is quite large. However, for thermosensible liquids, such as liquid nitrogen and liquid hydrogen, this approach is only approximate, and the error had to be accounted for by introducing the cavitation constants.

This work was supported by the National Basic Research Program of China (2011CB706501) and the Zhejiang Provincial Natural Science Foundation of China (Y12E060026).

1 Ashok K S, Mahesh M A, Li H Y, et al. Mathematical basis and validation of the full cavitation model. J Fluids Eng, 2002, 124: 617–624
2 Wu L, Lu C J, Li J, et al. Numerical simulations of 2D periodic unsteady cavitating flows. J Hydrol, 2006, 18: 341–344
3 Deshpande M, Feng J, Merkle C L. Numerical modeling of the thermodynamic effects of cavitation. J Fluids Eng, 1997, 119: 420–427
4 Ventikos Y, Tzabiras G. A numerical method for the simulation of steady and unsteady cavitating flows. Comput Fluids, 2000,29: 63–88
5 Saurel R, Cocchi J P, Butler P B. Numerical study of cavitation in the wake of a Hypervelocity under water projectile. J Propul Power, 1999, 15: 513–522
6 Tseng C C, Shyy W. Modeling for isothermal and cryogenic cavitation. Int J Heat Mass Tran, 2010, 53: 513–525
7 Senocak I, Shyy W. Interfacial dynamics-based modeling of turbulent cavitating flows, Part-1: Model development and steady- state computations. Int J Numer Meth Fluids, 2004, 44: 975–995
8 Hosangadi A, Ahuja V. Numerical study of cavitation in cryogenic fluids. J Fluids Eng, 2005, 127: 267–281
9 Zhang X B, Qiu L M, Gao Y, et al. Computational fluid dynamic study on cavitation in liquid nitrogen. Cryogenics, 2008, 48: 432–438
10 Cao X L, Zhang X B, Qiu L M. Validation of full cavitation model in cryogenic fluids. Chin Sci Bull, 2008, 54: 1633–1640
11 Wang G Y, Senocak I, Shyy W, et al. Dynamics of attached turbulent caviating flows. Prog Aerosp Sci, 2001, 37: 551–581
12 Wu J Y, Wang G, Shyy W. Time-dependent turbulent cavitating flow computations with interfacial transport and filter-based models. Int J Numer Meth Fl, 2005, 49: 739–761
13 Kunz R F, Boger D A, Stinebring D R, et al. A preconditioned Navier-Stokes method for two-phase flows with application to cavitation. Comput Fluids, 2000, 29: 849–875
14 Merkle C L, Feng J, Buelow P E O. Computational modeling of dynamics of sheet cavitation. In: Proc 3rd International Symposium on Cavitation, Grenoble, France, 1998
15 Zhang X B, Cao X L, Qiu L M. CFD study on cavitation of liquid oxygen in Venturi (in Chinese). CIESC J, 2009, 60: 1638–1643
16 Fluent6.3 documents, Fluent Incorporation, 2006
17 Hord J. Cavitation in Liquid Cryogens, II–hydrofoil, NASA Contractor Report, NASA CR-2156. 1973
18 Hord J. Cavitation in Liquid Cryogens, III–Ogive, NASA Contractor Report, NASA CR-2242. 1973
19 Ahuja V, Hosangadi A, Arunajatesan S. Simulations of cavitating flows using hybrid unstructured meshes. J Fluids Eng, 2001, 123: 331–340
20 Zhang X B, Qiu L M, Qi H, et al. Modeling liquid hydrogen cavitating flow with the full cavitation model. Int J Hydrogen Energ, 2008, 33: 7197–7206
21 Van P C. Liquid-Vapor Phase Change Phenomena: An Introduction to the Thermophysics of Vaporization and Condensation Processes in Heat Transfer Equipment, Washington: Hemisphere Publishing Corporation, 1992
22 Delale C F, Okita K, Matsumoto Y. Steady-state cavitating nozzle flows with nucleation. J Fluids Eng, 2005, 127: 770–777